Atmos. Chem. Phys. Discuss., https://doi.org/10.5194/acp-2018-790
Manuscript under review for journal Atmos. Chem. Phys.
Discussion started: 2 October 2018

Atmospheric Chemistry and Physics Discussions

The global climatology of the intensity of ionospheric sporadic *E* layer

Bingkun Yu[1,2], Xianghui Xue[1,2,3], Xin'an Yue[4], and Xiankang Dou[1,2]

[1]CAS Key Laboratory of Geospace Environment, Department of Geophysics and Planetary Sciences, University of Science and Technology of China, Hefei, China
[2]Mengcheng National Geophysical Observatory, School of Earth and Space Sciences, University of Science and Technology of China, Hefei, China
[3]Synergetic Innovation Center of Quantum Information and Quantum Physics, University of Science and Technology of China, Hefei, China
[4]Key Laboratory of Earth and Planetary Physics, Institute of Geology and Geophysics, Chinese Academy of Sciences, Beijing, China

Correspondence: Xianghui Xue (xuexh@ustc.edu.cn)

Abstract. On the basis of S4max data retrieved from COSMIC GPS radio occultation measurements, the long-term climatology of the intensity of E_s layers is investigated for the period from December 2006 to January 2014. The global maps of E_s intensity shows a high spatial resolution geographical distributions and strong seasonal dependence of E_s layers.The maximum intensity of E_s occurs in the midlatitudes, and its value in summer is 2–3 times larger than that in winter. A relatively strong E_s layer is observed at the North and South Poles with a distinct boundary dividing the middle latitudes and high latitudes along 60°–80° geomagnetic latitude bands. Besides, simulation results shows that the convergence of vertical ion velocity could partially explain the seasonal dependence of E_s intensity. Furthermore, some disagreements between the distributions of calculated divergence of vertical ion velocity and observed E_s intensity indicate that other processes such as magnetic field effects, meteoric mass influx into the earth's atmosphere and chemical processes of metallic ions should also be considered, which play an important role in the spatial and seasonal variations of E_s layers.

1 Introduction

The ionospheric sporadic *E* (E_s) layers are known as thin-layered structures of intense high electron density at 90–130 km altitudes. Rocket-borne mass spectrometric measurements proved that the E_s layer is mostly the ionization of metal atoms such as Fe^+, Mg^+, and Na^+ (Kopp, 1997; Grebowsky and Aikin, 2002). The E_s layer is mainly at midlatitudes and relatively absent at geomagnetic equator and high latitudes (Whitehead, 1989). It is widely accepted that the mechanism responsible for the E_s layer formation at midlatitudes is the windshear theory, in which the zonal and meridional winds provide the vertical windshear convergence nodes. As a result, the long-lived metallic ions are forced to converge towards the wind shear null to form a thin layer of intense metallic ionization(Whitehead, 1961; Macleod, 1966; Whitehead, 1970; Nygren et al., 1984; Whitehead, 1989; Haldoupis, 2012). In the equatoral region, the physical process of E_s irregularities is attributed to the gradient-drift instabilities associated with the equatorial electrojet (Tsunoda, 2008). The E_s layer generally has a vertical scale of 1 km or less, but its

Atmos. Chem. Phys. Discuss., https://doi.org/10.5194/acp-2018-790
Manuscript under review for journal Atmos. Chem. Phys.
Discussion started: 2 October 2018

Atmospheric Chemistry and Physics Discussions

horizontal scale can extend up to several hundreds of kilometers. Consequently, the intense E_s plasma irregularities and its sharp vertical electron density gradients seriously affect radio communications and navigation systems (Pavelyev et al., 2007). Furthermore, these effects on the GPS radio occultation (RO) signals detected by low Earth-orbit satellites can be exploited for lower atmospheric and ionospheric global investigations (Rocken et al., 2000; Hocke and Tsuda, 2001; Schreiner et al., 2007; Yue et al., 2010, 2011).

Observations of E_s layers were widely investigated from ground-based radars (e.g., Farley, 1985; Whitehead, 1989; Kelly, 1989; Chu and Wang, 1997; Mathews, 1998). In addition to ground-based radars, the scintillations of GPS RO were employed to extensively investigate the E_s layers over the past decades (Wu et al., 2005; Arras et al., 2008; Zeng and Sokolovskiy, 2010; Chu et al., 2011). A global map of E_s layers was first presented based on a meridian chain of ionosonde stations (Leighton et al., 1962). In recent years, on the basis of GPS RO measurements, the knowledge of global E_s layer occurrence rate, hereafter called E_sOR, has been advanced remarkably. Wu et al. (2005) used variances of the phase and signal-to-noise ratio (SNR) from ∼6000 GPS/CHAMP occultations to study the global climatology of E_sOR. Arras et al. (2008) investigated the global E_sOR distribution with a resolution of 5°×5° based on the CHAMP, GRACE (Gravity Recovery and Climate Experiment), and COSMIC (Constellation Observing System for Meteorology, Ionosphere, and Climate) occultation data. These previous studies of global E_sOR maps show a strong seasonal variation with the summer maximum in the middle latitudes. Chu et al. (2014) employed the COSMIC measurements to study the global morphology of E_sOR and the result of theoretical simulations suggested that the E_sOR seasonal variation is likely attributed to the convergence of metallic ion flux caused by the vertical wind shear. Shinagawa et al. (2017) calculated the global distribution of the vertical ion convergence and showed that the local and seasonal variations in the wind shear distribution could partially account for the geographical and seasonal variation of E_sOR.

There have been a lot of papers reporting the geographical distribution and seasonal variation of global E_s layers retrieved from GPS RO signals, and nearly all these works were on the occurrence rate of E_s layers. The purpose of the present paper is to study the global intensity of E_s layers, and compare the results of E_s intensity with the previous studies of E_sOR. The occurrence of E_s layers can cause both the SNR fluctuations and relative slant total electron content (TEC) peaks (Yue and Lyons, 2015). Sometimes the SNR has specific U-shape structures in the amplitude of GPS RO signals as reported by Zeng and Sokolovskiy (2010). The obvious increase of slant TEC occurring around 92 km implies the ionization enhancement in the E_s. In this study, the scintillation index (S4 index) data measured from SNR fluctuations of L1 channel of COSMIC GPS RO profiles at altitudes between 90 and 130 km for the period from December 2006 to January 2014 are employed to study the global climatology of the ionization of E_s layers. Section 2 describes the used data sets and procedure adopted to derive the S4 index. In Section 3, the global long-term behaviors of E_s layers with a high spatial resolution are presented and compared with the previous E_sOR results, including the latitude-day, latitude-longitude, altitude-latitude distribution, seasonal variations, and geomagnetic dependence of E_s layers. In section 4, on the basis of the windshear theory combined with several global-scale models, i.e., the Whole Atmosphere Community Climate Model (WACCM) (Marsh et al., 2013), the NRL Mass Spectrometer and Incoherent Scatter (MSIS)-00 atmospheric model (Picone et al., 2002), and the International Geomagnetic Reference Field (IGRF)-12 geomagnetic field model (Thébault et al., 2015), we calculate the global distribution of divergence of metallic ion

Atmos. Chem. Phys. Discuss., https://doi.org/10.5194/acp-2018-790
Manuscript under review for journal Atmos. Chem. Phys.
Discussion started: 2 October 2018

Atmospheric Chemistry and Physics Discussions

velocity to compare with the observations of E_s layers from COSMIC satellites. The magnetic declination angle effect on the divergence of metallic ion velocity in the simulation of E_s is investigated for the first time. The section 5 is the discussion and conclusions of this paper.

2 Data and Procedure of Deriving S4 index

The COSMIC global data sets used in this study are the COSMIC-GPS amplitude scintillation S4 indices. The GPS radio signal is received by the precise orbit determination antennas of COSMIC for each GPS RO when a GPS sets or rises behind earths' atmosphere as seen by the low-earth-orbit (LEO) satellite. Once the GPS signal received at LEO, the onboard algorithm of the GPS receiver measures SNR intensity fluctuations from the raw 50 Hz L1 amplitude measurements, which is then recorded in the data stream at 1 Hz rate at the ground receiver in order to minimize the data record size (Syndergaard et al., 2006). The raw scintillation measurement from the receiver is therefore the RMS of the SNR intensity fluctuation over one second, i.e., σ_I which can be expressed as: $\sigma_I = \sqrt{\langle (I - \langle I \rangle)^2 \rangle}$. I is the the square of the L1 SNR, and the bracket $\langle\rangle$ denotes the one second averaged value. The S4 indices are reconstructed by the COSMIC Data Analysis and Archive Center (CDAAC) ground processing after these σ_I data are downloaded (Rocken et al., 2000). During the procedure of deriving S4 indices, two additional steps are included in the ground processing. The first step is to assume the SNR intensity fluctuations have Gaussian distributions so as to calculate an approximate value of $\langle I \rangle$ from σ_I and $\langle \mathrm{SNR} \rangle$. The second is to apply a low pass filter to the time serious of $\langle I \rangle$ to get a new average of the intensity $\langle I \rangle_{new}$ at each second to replace the $\langle I \rangle$ in the calculation of S4 indices. After these steps, a long-term detrended S4 scintillation index can be reconstructed by the CDAAC ground processing. Further details on the procedure of deriving S4 index along with some individual example figures can be found in the report of Ko and Yeh (2010).

In the present study, the COSMIC global data sets specifically denote the maximum value of S4 (S4max). The COSMIC global S4max data include the S4max value, geographic latitude, longitude, altitude as well as local time on which the S4max was detected. The computed detrended S4max index is available from 28 December 2006 onwards in the CDAAC website (http://cdaac-www.cosmic.ucar.edu/cdaac). The long-term global climatology of the E_s intensity is investigated based on the global S4max data from December 2006 to January 2014. Figure 1 shows the altitude distribution of COSMIC S4max profiles. A considerable numbers of profiles are distributed at altitudes between 40 and 130 km with a peak number at around 100 km. Information on E_s layers can be extracted from amplitude fluctuations in the SNR profiles (Wu et al., 2005). Please note that as a result of the integral influence either in the SNR or the slant TEC along the LEO-GPS ray, the effect of E_s layers in the high altitudes could map down to the lower tangent point altitudes, which may induce pseudo multiple peaks in one RO event (Zeng and Sokolovskiy, 2010). In Figure 1, the occurrence of sporadic E can be seen down to 40 km as a result of the localization problem of RO measurement. In fact, E_s layers could not be formed by the wind shear theory below 90 km because of the high ion-neutral collision frequencies. The E_s layer over the lower altitude should be some artefact resulting from mapping effect. Therefore, the S4max values which appear in the altitude range between 90 and 130 km are used to study the E_s layers in the

Atmos. Chem. Phys. Discuss., https://doi.org/10.5194/acp-2018-790
Manuscript under review for journal Atmos. Chem. Phys.
Discussion started: 2 October 2018

Atmospheric Chemistry and Physics Discussions

lower ionosphere region. The global morphology of the E_s intensity is presented and its altitude and seasonal dependences are given at a high spatial resolution because of the large COSMIC RO data sets with a high vertical resolution.

3 Observations

Figure 2 shows long-term time series of the E_s values with a resolution of 5° latitudes × 5 days. As shown, the E_s layer is mainly a sporadic layered phenomenon in the summer hemisphere as is known from former E_sOR studies (Leighton et al., 1962; Wu, 2006; Arras et al., 2008; Chu et al., 2014). In Figure 2, it is clear that the intensity of E_s is enhanced in the northern (southern) summer hemisphere from May to September (from November to March), with maximum in June (December), i.e., one month ahead of E_sOR maximum (Chu et al., 2014). In addition, the seasonal E_s layer also has an interannual variability. Compared with the intense Es activity in the 2010 and 2011 summers, the intensity of E_s is lower in the 2012 and 2013 northern summers. It may be caused by anomalies of wind fields in the upper atmosphere and a corresponding reduction of vertical windshear associated with E_s formation.

The map in Figure 3 shows the global geographical distributions of E_s values with a significantly improved spatial resolution of a 1°× 1° grid. The red and green solid curves represent the northern and southern geomagnetic latitude contours of 60°, 70°, 80°, respectively. The geomagnetic equator is also plotted in a yellow curve. The E_s layers dominantly distribute with S4max value exceeding 0.7 in the middle latitudes. Because of the increased spatial resolution, the regional features and longitudinal variations become visible. The intensity of E_s is much weaker in the lower latitudes of both hemispheres, especially a noticeable gap near the magnetic equator. It could be explained by the vanishing vertical component of the geomagnetic field lines which keep the ionized particles from effectively vertically converging. Furthermore, the E_s longitudinal variations of the geomagnetic field are also clearly shown. The decrease of the E_s intensity can be seen clearly in the Southern Atlantic Anomaly (SAA) zone and the northern American region with dependence of geomagnetic latitudes. The region of large E_s intensity exists in the Northern Africa and North Atlantic regions, Southeast Asian region, Southern Africa and South Pacific regions. A difference between the E_s intensity and E_sOR distributions is in the high latitudes, that is, the occurrence rates of E_s is generally low (Arras et al., 2008) but the intensity of E_s is relatively high. It appears more evident in the magnetic poles, likely as a result of intense solar activities. The lower panels depicts the northern and southern polar views of distributions of E_s values, and these views make the signature more clear.

The maps in Figure 4 show the geographical distribution of E_s intensity for four different seasons in a 1°× 1° grid. The distribution of E_s layers shows a significant seasonal dependence. The intensity of E_s layers in the middle latitudes of the summer hemisphere is 2–3 times larger than that in the winter hemisphere. During equinox seasons, the intensity of E_s layers is moderate covering around the globe and a distinct boundary dividing the middle latitudes and high latitudes is visible along 60°–80° geomagnetic latitude bands. From the polar views of each season, it can be seen that the E_s layers remain in a relatively high level at the North and South Poles. It could be attributed to the high energy radiation and particle precipitations. The ionization of E_s layers is persistently magnetic fields trapped in the polar regions.

Atmos. Chem. Phys. Discuss., https://doi.org/10.5194/acp-2018-790
Manuscript under review for journal Atmos. Chem. Phys.
Discussion started: 2 October 2018

Atmospheric Chemistry and Physics Discussions

Figure 5 shows the altitude-latitude distribution of the E_s intensity with a resolution of 1 km altitude $\times$ 1° latitude. The intensity of E_s distributes at altitudes between 95 and 125 km. The most dense patches of E_s exist at altitudes exceeding 110 km. It is different from the E_sOR altitude-latitude distribution which dominates at 95–110 km with the peak around 105 km in the middle latitudes of 25°–45°(Arras et al., 2008). The E_s intensity has a broader latitudinal extent of 10°S–75°S in the Southern Hemisphere, compared with 10°N–60°N in the Northern Hemisphere.

Figure 6 presents the seasonal variation in the altitude-latitude distributions of the E_s intensity for the same temporal period and same spatial resolution as in Figure 5. It is clearly that, the E_s intensity for the summer and winter solstices has a significantly broader latitudinal extent to the high latitude region. Besides, the overall intensity of E_s layers increases spanning a larger vertical extent during solstices. In general, the E_s intensity exceeding 0.65 values distributes at altitudes of 100–125 km in southern summer and at altitudes of 90–130 km in northern summer. During equinox seasons, the E_s intensity is moderate and its altitude-latitude distribution is relatively symmetric.

4 Wind Shear Theory Explanation for E_s Seasonal Variation

The global climatology of the intensity of E_s layers is investigated from the COSMIC occultation data employing the GPS RO technique. One of the pronounced variability in E_s layers is the seasonal variation with maximum appearing in the summer hemisphere. Although the mechanism for the E_s layer formation is widely accepted that these dense and thin layers of metallic ion plasma are formed by the vertical ion convergence of neutral wind shear. The overall morphology of E_s layers cannot be explained by the windshear theory. One of the unsolved issues in the ionosphere is that the well pronounced seasonal dependence of mid-latitude E_s layers does not have a comprehensive explanation, which is inexplicable from the windshear theory (Whitehead, 1989; Haldoupis et al., 2007).

The seasonal dependence is found not only in the E_s intensity but also in the former studies of E_sOR variations (Wu et al., 2005; Arras et al., 2008; Chu et al., 2014). Chu et al. (2014) simulated the global distribution of the convergence of metallic ion flux caused by the vertical wind shear, suggesting the maximum of E_s in summer and minimum of E_s in winter are likely caused by the vertical windshear effect.

From the wind shear theory (e.g., Nygren et al., 1984; Mathews, 1998; Kirkwood and Nilsson, 2000), the vertical Fe^+ ion velocity w_i induced by the neutral wind is described by equation (1):

$$w_i = \frac{r_i cosI}{1+r_i^2} \times U - \frac{sinIcosI}{1+r_i^2} \times V + \frac{r_i^2 + sin^2 I}{1+r_i^2} \times W \quad (1)$$

where I is the magnetic inclination angle that is defined positive (downward direction) in Northern Hemisphere, r_i is the ratio of the ion-neutral collision frequency (ν_i) to the ion gyrofrequency (ω_i), and neutral wind velocity V_n=(U, V, W) components are zonal (positive for eastward), meridional (positive for northward), and vertical (positive upward) directions. Therefore, the favorable wind field for E_s layer formation is where there is a negative $\frac{dw_i}{dz}$, indicating an ion-convergence region.

Our study has the following simulations of global distribution of divergence of ion velocity in comparison with previous studies. The neutral wind is provided by output from WACCM and the ion-neutral frequency is calculated by the atmospheric

Atmos. Chem. Phys. Discuss., https://doi.org/10.5194/acp-2018-790
Manuscript under review for journal Atmos. Chem. Phys.
Discussion started: 2 October 2018

Atmospheric Chemistry and Physics Discussions

composition from MSIS-00 atmospheric model in accordance with Chu et al. (2014). The global distributions of geomagnetic field and magnetic inclination angle at 100 km are estimated from IGRF-12 model. The calculation of ion velocity is binned and averaged in a 1° latitude × 1° longitude grid at WACCM altitude levels from 0–130 km.

Figure 7 presents simulation results of the global distributions of the monthly mean divergence of vertical ion velocity in the altitude range between 97 and 114 km in January and July. The negative (positive) $\frac{\mathrm{d}w_i}{\mathrm{d}z}$ represents convergence (divergence) of the Fe^+ ion in units of $ms^{-1}km^{-1}$. It shows a good correlation between the simulated distributions of monthly mean divergence of vertical ion velocity in Figure 7 and the geographical distribution of E_s intensity measured from the COSMIC GPS RO profiles in Figure 4. Chu et al. (2014) simulated the global distributions of the mean divergence of the Fe^+ concentration flux at altitudes of 94–115 km for four seasons. It also showed a similar simulation result of distributions of divergence of the Fe^+ concentration flux, which is well correlated with the COSMIC-measured E_sOR distribution. The simulation of divergence of vertical ion velocity supports the wind shear theory for the E_s formation and also indicates the seasonal dependence of E_s layers is likely attributed to the convergence of vertical ion velocity driven by the neutral wind.

Furthermore, we also notice that the E_s intensity distributes at relatively higher altitudes of 95–125 km compared with E_sOR at 90–120 km. The most dense patches of E_s exit above 115 km, and the E_s layer has a broader vertical extent in summer as shown in Figure 5 and Figure 6. In the simulation, the distributions of the monthly mean divergence of vertical ion velocity in the altitude range of 114–128 km in January and July are shown in Figure 8. In contrast to the distributions of the divergence of vertical ion velocity between 97 and 114 km in Figure 7, Figure 8 shows an ion-divergence region at altitudes of 114–128 km in summer at midlatitudes as a result of different zonal and meridional winds. It suggests that a single windshear theory likely has difficulty in explaining the E_s layer formation at higher altitudes.

In previous studies of the windshear theory for the E_s layer formation, the magnetic declination angle effect is neglected in the calculation of the vertical ion velocity w_i induced by the neutral wind. The steady-state ion momentum equation is:

$$m\frac{\mathrm{d}\boldsymbol{v}_i}{\mathrm{d}t} = 0 = e(\boldsymbol{E} + \boldsymbol{v}_i \times \boldsymbol{B}) - M\nu_{in}(\boldsymbol{v}_i - \boldsymbol{V}_n) \tag{2}$$

On the basis of the steady-state ion momentum equation, the euqation (1) of vertical ion velocity w_i is extended to take the magnetic declination angle D into consideration as follows:

$$w_i = \frac{r_i cosDcosI - sinDsinIcosI}{1 + r_i^2} \times U - \frac{r_i sinDcosI + cosDsinIcosI}{1 + r_i^2} \times V + \frac{r_i^2 + sin^2 I}{1 + r_i^2} \times W \tag{3}$$

The magnetic declination angle currently ranges from -30° (west) to 26° (east). The magnetic declination angle effect on the divergence of ion velocity in the simulation of E_s is investigated. Figure 9 presents the global distributions of the monthly mean divergence of vertical ion velocity in the altitude range of 97–114 km with the consideration of the magnetic declination angle. It shows a seasonal dependence with ion-convergence regions in summer and ion-divergence regions in winter. However, the morphology of the divergence of vertical ion velocity is different from that without the magnetic declination angle considered shown in Figure 7. In January, the strong ion convergence appears in the SAA region. In July, the Asia and Europe, and North Pacific tend to be the regions of ion convergence.

Atmos. Chem. Phys. Discuss., https://doi.org/10.5194/acp-2018-790
Manuscript under review for journal Atmos. Chem. Phys.
Discussion started: 2 October 2018

Atmospheric Chemistry and Physics Discussions

5 Discussion

The seasonal and geographical dependences of E_sOR have been widely studied by ionospheric observations since 1960s (Leighton et al., 1962; Smith, 1978; Wu et al., 2005; Arras et al., 2008; Zeng and Sokolovskiy, 2010), but so far the overall morphology of E_s is still not well explained. The seasonal dependence of E_s layers remains a long-going mystery as it is unexpected in the classical windshear theory reported in the review paper of Whitehead (1989). In recent time, Chu et al. (2014) simulated the distribution of the convergence of the Fe^+ concentration flux and indicated that the vertical ion convergence caused by neutral wind could be responsible for the seasonal dependence of E_s.

In our investigations, it is found that the intensity of E_s layers has a seasonal dependence with a pronounced maximum in the midlatitudes in the summer hemisphere as shown in Figure 4. The E_s intensity has a similar seasonal and spatial distributions to E_sOR, but the E_s layer has a relatively large intensity and a small E_sOR value at the North and South Poles. The strong E_s layers in the Earth's polar regions could be caused by the solar energetic particles and cosmic rays.

On the other hand, the simulation of the global distributions of the monthly mean divergence of vertical ion velocity shows an ion-convergence region in the summer midlatitudes, which is similar to the simulation results of Chu et al. (2014). It suggests that the seasonal dependence of E_s is likey attributed to the vertical convergence of ions driven by the neutral wind. However, some disagreements between the distributions of calculated divergence of vertical ion velocity and observed E_s intensity are found. For example, there are ion-divergence regions in the midlatitudes in winter in Figure 7, but the dissipation of E_s is observed in the 60°–80° geomagnetic latitude bands. The most dense E_s layer appears above 115 km higher than E_sOR. Another discrepancy is that the simulated divergence of vertical ion velocity in the altitude range between 114 and 128 km has a positive $\frac{\mathrm{d}w_i}{\mathrm{d}z}$ in the summer hemisphere. It indicates an ion-divergence region of ions in contrast to the observed summer maximum of E_s intensity in the summer midlatitudes.

The magnetic declination angle effect on the divergence of metallic ion velocity is investigated in the simulation of E_s for the first time in Figure 9. Though it shows the marked seasonal dependence with a strong summer ion-convergence region, the morphology of the divergence of vertical ion velocity is different from the distribution of observed E_s intensity in Figure 7. Thus, the vertical ion convergence by itself is far from sufficient to explain the strong E_s summer maximum. Some other physical processes should also be considered in the geographical distribution and spatial variations in E_s layers which play important roles in determining the global morphology of E_s such as the magnetic field, ionospheric electric field, chemical processes of metallic ions, large geomagnetic storms, and meteorological processes in the lower atmosphere (e.g., Mathews, 1998; Carter and Forbes, 1999; Davis and Johnson, 2005; Johnson and Davis, 2006; Haldoupis, 2012; Yue et al., 2012; Feng et al., 2013; Yu et al., 2015)

Haldoupis et al. (2007) proposed the seasonal dependence of E_s could be explained by the seasonal variation of the meteor influx into the upper atmosphere. However, it has been largely accepted now that sporadic meteoroids provides a extremely greater meteor mass on average than meteor showers (Ceplecha et al., 1998; Baggaley, 2002; Janches et al., 2002; Williams and Murad, 2002). The meteoric mass influx caused by sporadic meteoroids reaches a maximum in autumn rather than summer (Janches et al., 2006). It is well established that the global input of meteoric material gives rise to the mesospheric metal layers

Atmos. Chem. Phys. Discuss., https://doi.org/10.5194/acp-2018-790
Manuscript under review for journal Atmos. Chem. Phys.
Discussion started: 2 October 2018

Atmospheric Chemistry and Physics Discussions

and E_s layers (Plane, 2004; Carrillo-Sánchez et al., 2015; Plane et al., 2015), but the daily amount is still not well defined and estimates of the global Interplanetary Dust Particles (IDP) range from 5–270 tonnes per day (Plane, 2012). These effects of meteoric ablation are significantly influenced by the magnitude of the IDP input by two orders of magnitude uncertainty. On the other hand, this fact also highlights the importance of the fundamental understanding in the global climatology of E_s layers.

6 Conclusions

In this study, we investigate the long-term climatology of the intensity of E_s layers on the basis of S4max data retrieved from COSMIC GPS RO measurements. The resulting global E_s maps with a high spatial resolution presents geographical distributions and strong seasonal dependence of E_s intensity, which is consistent with former studies of global E_sOR maps (Wu, 2006; Arras et al., 2008; Chu et al., 2014). The high E_s intensity in summer exists at altitudes of 115-125 km in the 10°–60° latitudes in the Northern Hemisphere, and at altitudes of 115-120 km in the 10°–75° latitudes in the Southern Hemisphere.

Furthermore, simulation results of the global distributions of the monthly mean divergence of vertical ion velocity could partially explain the seasonal dependence of E_s intensity. The magnetic declination angle effect on the divergence of metallic ion velocity in the simulation of E_s is investigated, and we discuss some disagreements between the distributions of calculated divergence of vertical ion velocity and observed E_s intensity. It indicates that, in addition to the vertical windshear effects, other processes such as magnetic field effects, meteoric mass influx into the earth's atmosphere and chemical processes of metallic ions are also likely to play an dominant role in the geographical and seasonal variations of E_s layers.

Competing interests. The authors declare that they have no conflict of interest.

Acknowledgements. We acknowledge the COSMIC radio occultation data as well as the WACCM, NRL MSIS-00 atmospheric model and IGRF-12 geomagnetic field model data used in this paper. This work is supported by the National Natural Science Foundation of China (41774158, 41474129, 41421063), the open research project of CAS Large Research Infrastructures, the Youth Innovation Promotion Association of the Chinese Academy of Sciences (2011324) and the Fundamental Research Fund for the Central Universities.

Atmos. Chem. Phys. Discuss., https://doi.org/10.5194/acp-2018-790
Manuscript under review for journal Atmos. Chem. Phys.
Discussion started: 2 October 2018

Atmospheric Chemistry and Physics Discussions

References

Arras, C., Wickert, J., Beyerle, G., Heise, S., Schmidt, T., and Jacobi, C.: A global climatology of ionospheric irregularities derived from GPS radio occultation, Geophysical research letters, 35, 2008.

Baggaley, W. J.: Radar observations, Meteors in the Earth's Atmosphere, pp. 123–148, 2002.

Carrillo-Sánchez, J., Plane, J., Feng, W., Nesvornỳ, D., and Janches, D.: On the size and velocity distribution of cosmic dust particles entering the atmosphere, Geophysical research letters, 42, 6518–6525, 2015.

Carter, L. and Forbes, J.: Global transport and localized layering of metallic ions in the upper atmosphere, 17, 190–209, 1999.

Ceplecha, Z., Borovička, J., Elford, W. G., ReVelle, D. O., Hawkes, R. L., Porubčan, V., and Šimek, M.: Meteor phenomena and bodies, Space Science Reviews, 84, 327–471, 1998.

Chu, Y., Wang, C., Wu, K., Chen, K., Tzeng, K., Su, C., Feng, W., and Plane, J.: Morphology of sporadic E layer retrieved from COSMIC GPS radio occultation measurements: Wind shear theory examination, Journal of Geophysical Research: Space Physics, 119, 2117–2136, 2014.

Chu, Y.-H. and Wang, C.-Y.: Interferometry observations of three-dimensional spatial structures of sporadic E irregularities using the Chung-Li VHF radar, Radio Science, 32, 817–832, 1997.

Chu, Y.-H., Brahmanandam, P., Wang, C.-Y., Su, C.-L., and Kuong, R.-M.: Coordinated sporadic E layer observations made with Chung-Li 30 MHz radar, ionosonde and FORMOSAT-3/COSMIC satellites, Journal of Atmospheric and Solar-Terrestrial Physics, 73, 883–894, 2011.

Davis, C. J. and Johnson, C.: Lightning-induced intensification of the ionospheric sporadic E layer, Nature, 435, 799, 2005.

Farley, D.: Theory of equatorial electrojet plasma waves-new developments and current status, Journal of Atmospheric and Terrestrial Physics, 47, 729–744, 1985.

Feng, W., Marsh, D. R., Chipperfield, M. P., Janches, D., Höffner, J., Yi, F., and Plane, J.: A global atmospheric model of meteoric iron, Journal of Geophysical Research: Atmospheres, 118, 9456–9474, 2013.

Grebowsky, J. M. and Aikin, A. C.: In Situ Measurements of Meteoric Ions, Meteors in the Earth's Atmosphere, pp. 189–214, 2002.

Haldoupis, C.: Midlatitude sporadic E. A typical paradigm of atmosphere-ionosphere coupling, Space science reviews, 168, 441–461, 2012.

Haldoupis, C., Pancheva, D., Singer, W., Meek, C., and MacDougall, J.: An explanation for the seasonal dependence of midlatitude sporadic E layers, Journal of Geophysical Research: Space Physics, 112, 2007.

Hocke, K. and Tsuda, T.: Gravity waves and ionospheric irregularities over tropical convection zones observed by GPS/MET radio occultation, Geophysical Research Letters, 28, 2815–2818, 2001.

Janches, D., Pellinen-Wannberg, A., Wannberg, G., Westman, A., Häggström, I., and Meisel, D. D.: Tristatic observations of meteors using the 930 MHz European Incoherent Scatter radar system, Journal of Geophysical Research: Space Physics, 107, 2002.

Janches, D., Heinselman, C. J., Chau, J. L., Chandran, A., and Woodman, R.: Modeling the global micrometeor input function in the upper atmosphere observed by high power and large aperture radars, Journal of Geophysical Research: Space Physics, 111, 2006.

Johnson, C. and Davis, C. J.: The location of lightning affecting the ionospheric sporadic-E layer as evidence for multiple enhancement mechanisms, Geophysical research letters, 33, 2006.

Kelly, M. C.: The Earth's ionosphere, Int. Geophys. Ser, 43, 71, 1989.

Kirkwood, S. and Nilsson, H.: High-latitude sporadic-E and other thin layers–the role of magnetospheric electric fields, Space Science Reviews, 91, 579–613, 2000.

Ko, C. and Yeh, H.: COSMIC/FORMOSAT-3 observations of equatorial F region irregularities in the SAA longitude sector, Journal of Geophysical Research: Space Physics, 115, 2010.

Kopp, E.: On the abundance of metal ions in the lower ionosphere, Journal of Geophysical Research: Space Physics, 102, 9667–9674, 1997.

Leighton, H., Shapley, A., and Smith, E.: The occurrence of sporadic E during the IGY, in: Ionospheric Sporadic, pp. 166–177, Elsevier, 1962.

Macleod, M. A.: Sporadic E theory. I. Collision-geomagnetic equilibrium, Journal of the Atmospheric Sciences, 23, 96–109, 1966.

Marsh, D. R., Mills, M. J., Kinnison, D. E., Lamarque, J.-F., Calvo, N., and Polvani, L. M.: Climate change from 1850 to 2005 simulated in CESM1 (WACCM), Journal of climate, 26, 7372–7391, 2013.

Mathews, J.: Sporadic E: current views and recent progress, Journal of atmospheric and solar-terrestrial physics, 60, 413–435, 1998.

Nygren, T., Jalonen, L., Oksman, J., and Turunen, T.: The role of electric field and neutral wind direction in the formation of sporadic E-layers, Journal of Atmospheric and Terrestrial Physics, 46, 373–381, 1984.

Pavelyev, A., Liou, Y., Wickert, J., Schmidt, T., Pavelyev, A., and Liu, S.-F.: Effects of the ionosphere and solar activity on radio occultation signals: Application to CHAllenging Minisatellite Payload satellite observations, Journal of Geophysical Research: Space Physics, 112, 2007.

Picone, J., Hedin, A., Drob, D. P., and Aikin, A.: NRLMSISE-00 empirical model of the atmosphere: Statistical comparisons and scientific issues, Journal of Geophysical Research: Space Physics, 107, 2002.

Plane, J.: A time-resolved model of the mesospheric Na layer: constraints on the meteor input function, Atmospheric Chemistry and Physics, 4, 627–638, 2004.

Plane, J. M.: Cosmic dust in the Earth's atmosphere, Chemical Society Reviews, 41, 6507–6518, 2012.

Plane, J. M., Feng, W., and Dawkins, E. C.: The mesosphere and metals: Chemistry and changes, Chemical reviews, 115, 4497–4541, 2015.

Rocken, C., Ying-Hwa, K., Schreiner, W. S., Hunt, D., Sokolovskiy, S., and McCormick, C.: COSMIC system description, Terrestrial Atmospheric and Oceanic Sciences, 11, 21–52, 2000.

Schreiner, W., Rocken, C., Sokolovskiy, S., Syndergaard, S., and Hunt, D.: Estimates of the precision of GPS radio occultations from the COSMIC/FORMOSAT-3 mission, Geophysical Research Letters, 34, 2007.

Shinagawa, H., Miyoshi, Y., Jin, H., and Fujiwara, H.: Global distribution of neutral wind shear associated with sporadic E layers derived from GAIA, Journal of Geophysical Research: Space Physics, 122, 4450–4465, 2017.

Smith, E. K.: Temperate zone sporadic-E maps (?0Es> 7 MHz), Radio Science, 13, 571–575, 1978.

Syndergaard, S., Schreiner, W., Rocken, C., Hunt, D., and Dymond, K.: Preparing for COSMIC: Inversion and analysis of ionospheric data products, in: Atmosphere and Climate, pp. 137–146, Springer, 2006.

Thébault, E., Finlay, C. C., Beggan, C. D., Alken, P., Aubert, J., Barrois, O., Bertrand, F., Bondar, T., Boness, A., Brocco, L., et al.: International geomagnetic reference field: the 12th generation, Earth, Planets and Space, 67, 79, 2015.

Tsunoda, R. T.: On blanketing sporadic E and polarization effects near the equatorial electrojet, Journal of Geophysical Research: Space Physics, 113, 2008.

Whitehead, J.: The formation of the sporadic-E layer in the temperate zones, Journal of Atmospheric and Terrestrial Physics, 20, 49–58, 1961.

Whitehead, J.: Production and prediction of sporadic E, Reviews of Geophysics, 8, 65–144, 1970.

Whitehead, J.: Recent work on mid-latitude and equatorial sporadic-E, Journal of Atmospheric and Terrestrial Physics, 51, 401–424, 1989.

Williams, I. P. and Murad, E.: Meteors in the Earth's Atmosphere, Cambridge University Press, Cambridge, 2002.

Wu, D. L.: Small-scale fluctuations and scintillations in high-resolution GPS/CHAMP SNR and phase data, Journal of atmospheric and solar-terrestrial physics, 68, 999–1017, 2006.

Wu, D. L., Ao, C. O., Hajj, G. A., de La Torre Juarez, M., and Mannucci, A. J.: Sporadic E morphology from GPS-CHAMP radio occultation, Journal of Geophysical Research: Space Physics, 110, 2005.

Yu, B., Xue, X., Lu, G., Ma, M., Dou, X., Qie, X., Ning, B., Hu, L., Wu, J., and Chi, Y.: Evidence for lightning-associated enhancement of the ionospheric sporadic E layer dependent on lightning stroke energy, Journal of Geophysical Research: Space Physics, 120, 9202–9212, 2015.

Yue, J. and Lyons, W. A.: Structured elves: Modulation by convectively generated gravity waves, Geophysical Research Letters, 42, 1004–1011, 2015.

Yue, J., Wang, W., Richmond, A. D., and Liu, H.-L.: Quasi-two-day wave coupling of the mesosphere and lower thermosphere-ionosphere in the TIME-GCM: Two-day oscillations in the ionosphere, Journal of Geophysical Research: Space Physics, 117, 2012.

Yue, X., Schreiner, W. S., Lei, J., Rocken, C., Hunt, D. C., Kuo, Y.-H., and Wan, W.: Global ionospheric response observed by COSMIC satellites during the January 2009 stratospheric sudden warming event, Journal of Geophysical Research: Space Physics, 115, 2010.

Yue, X., Schreiner, W. S., Hunt, D. C., Rocken, C., and Kuo, Y.-H.: Quantitative evaluation of the low Earth orbit satellite based slant total electron content determination, Space Weather, 9, 2011.

Zeng, Z. and Sokolovskiy, S.: Effect of sporadic E clouds on GPS radio occultation signals, Geophysical Research Letters, 37, 2010.

Atmos. Chem. Phys. Discuss., https://doi.org/10.5194/acp-2018-790
Manuscript under review for journal Atmos. Chem. Phys.
Discussion started: 2 October 2018

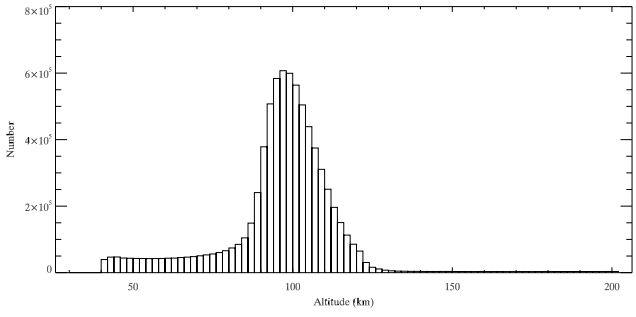

Figure 1. The altitude distribution of COSMIC S4max profiles from December 2006 to January 2014.

Atmos. Chem. Phys. Discuss., https://doi.org/10.5194/acp-2018-790
Manuscript under review for journal Atmos. Chem. Phys.
Discussion started: 2 October 2018

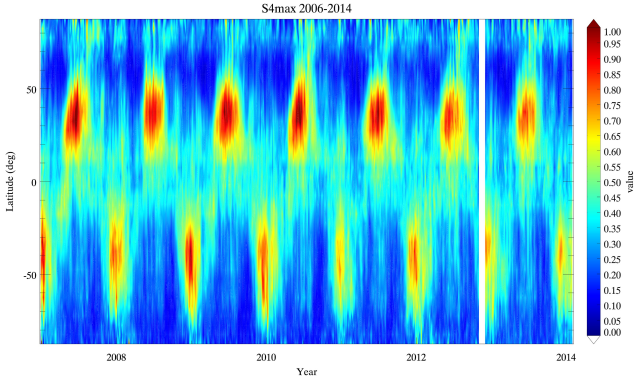

Figure 2. Time series of the E_s values with a resolution of 5° latitudes × 5 days for the period from December 2006 to January 2014.

Atmos. Chem. Phys. Discuss., https://doi.org/10.5194/acp-2018-790
Manuscript under review for journal Atmos. Chem. Phys.
Discussion started: 2 October 2018

Atmospheric Chemistry and Physics Discussions

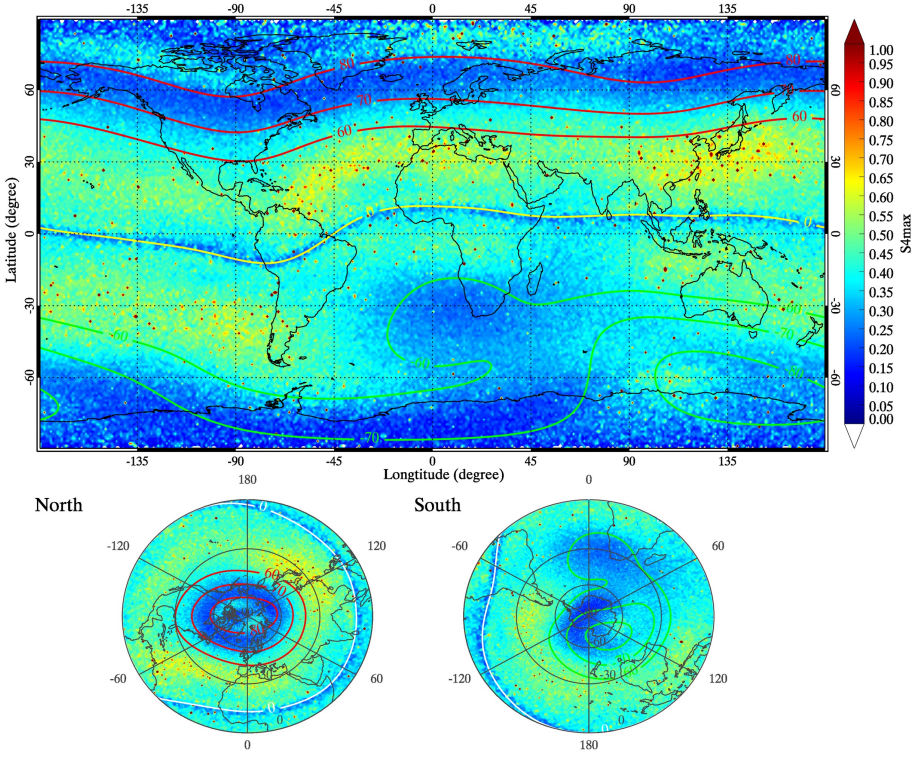

Figure 3. Global geographical distributions of E_s values with a spatial resolution of a $1^\circ \times 1^\circ$ grid. Red and green curves signify geomagnetic latitude contours of 60°, 70°, 80° and the yellow curve represents the geomagnetic equator.

Atmos. Chem. Phys. Discuss., https://doi.org/10.5194/acp-2018-790
Manuscript under review for journal Atmos. Chem. Phys.
Discussion started: 2 October 2018

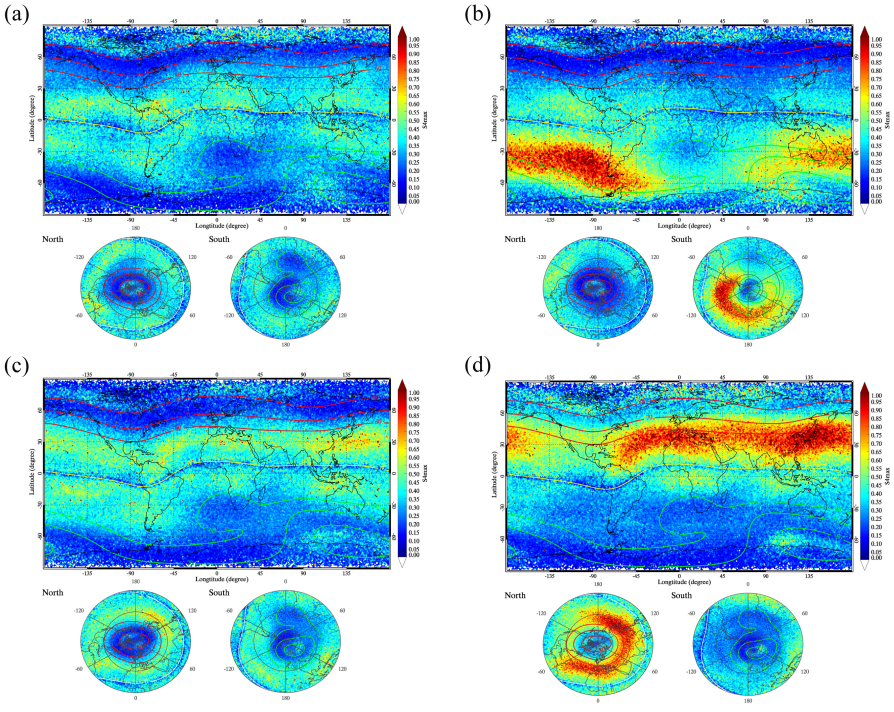

Figure 4. Seasonal variations of E_s intensity with a spatial resolution of a $1^\circ \times 1^\circ$ grid. Plots for the (top left) autumn (September, October, November), (top right) winter (December, January, February), (bottom left) spring (March, April, May), (bottom right) summer (June, July, August).

Atmos. Chem. Phys. Discuss., https://doi.org/10.5194/acp-2018-790
Manuscript under review for journal Atmos. Chem. Phys.
Discussion started: 2 October 2018

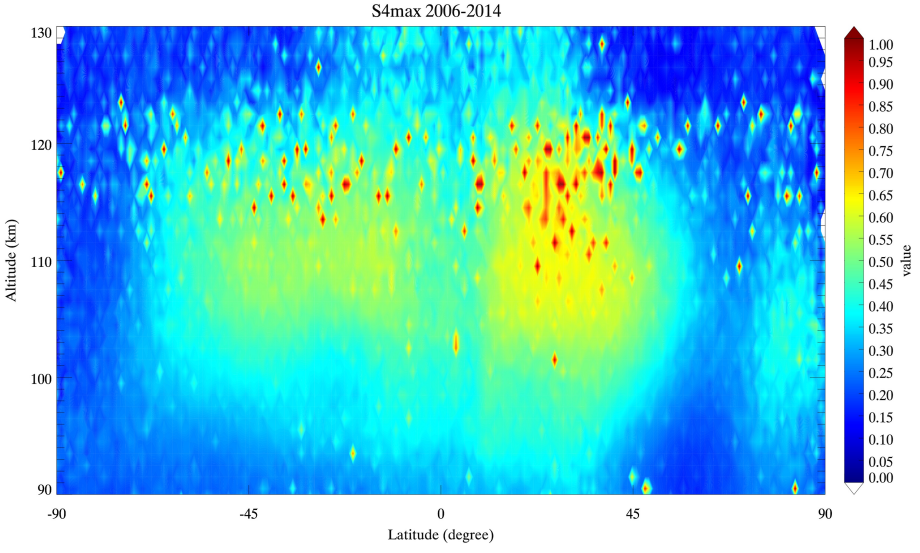

Figure 5. Altitude-latitude distribution of the E_s intensity with a resolution of 1 km altitude $\times$ 1° latitude.

Atmos. Chem. Phys. Discuss., https://doi.org/10.5194/acp-2018-790
Manuscript under review for journal Atmos. Chem. Phys.
Discussion started: 2 October 2018

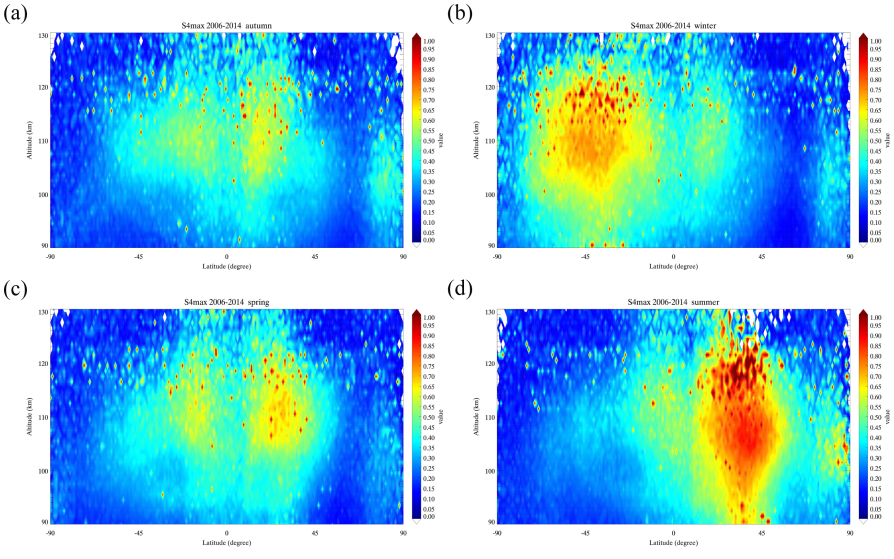

Figure 6. Seasonal variation in altitude-latitude distributions of the E_s intensity for four different seasons: (a) autumn, (b) winter, (c) spring, and (d) summer.

Atmos. Chem. Phys. Discuss., https://doi.org/10.5194/acp-2018-790
Manuscript under review for journal Atmos. Chem. Phys.
Discussion started: 2 October 2018

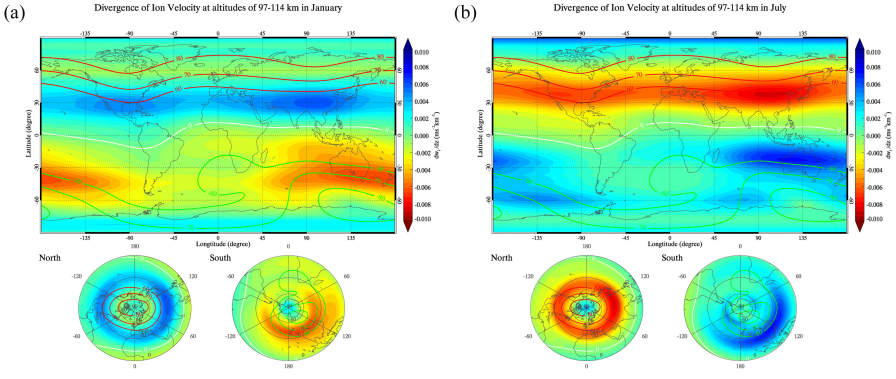

Figure 7. Simulation results of the global distributions of the monthly mean divergence of vertical ion velocity (in units of $ms^{-1}km^{-1}$) in the altitude range between 97 and 114 km in January (a) and July (b). Red and green curves signify 60°, 70°, 80° geomagnetic latitude contours and the yellow curve represents the geomagnetic equator.

Atmos. Chem. Phys. Discuss., https://doi.org/10.5194/acp-2018-790
Manuscript under review for journal Atmos. Chem. Phys.
Discussion started: 2 October 2018

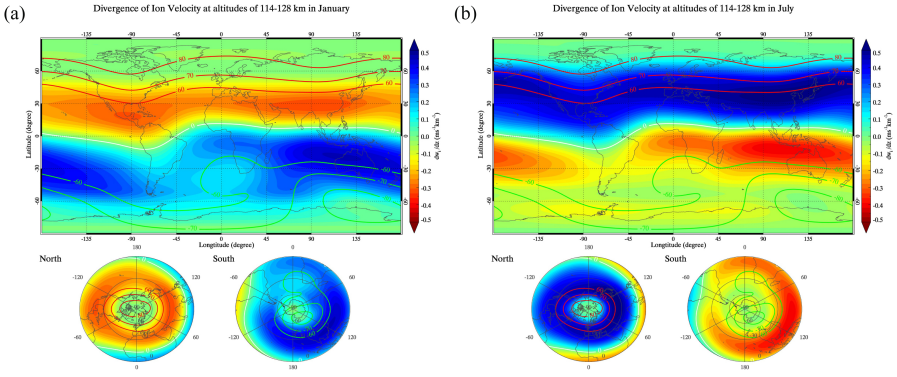

Figure 8. Same as figure 7 but for the altitude range between 114 and 128 km in January (a) and July (b).

Atmos. Chem. Phys. Discuss., https://doi.org/10.5194/acp-2018-790
Manuscript under review for journal Atmos. Chem. Phys.
Discussion started: 2 October 2018

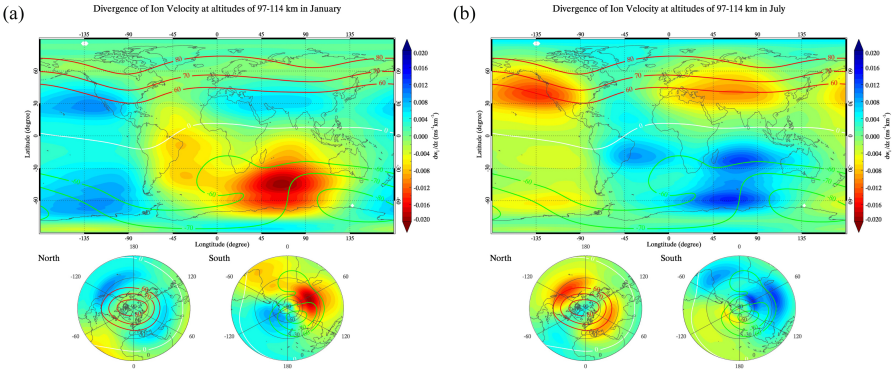

Figure 9. Same as figure 7 but for the consideration of the magnetic declination angle effect on the vertical ion velocity in January (a) and July (b).